

Computational analyses of transcriptomic data reveal the dynamic organization of the *Escherichia coli* chromosome under different conditions

Qin Ma¹, Yanbin Yin², Mark A. Schell¹, Han Zhang³, Guojun Li^{1,4} and Ying Xu^{1,5,6,*}

¹Computational Systems Biology Laboratory, Department of Biochemistry and Molecular Biology and Institute of Bioinformatics, University of Georgia, Athens, GA 30602, USA, ²Department of Biological Sciences, Northern Illinois University, DeKalb, IL 60115-2857, USA, ³Department of Automation and Intelligent Science, College of Information Technical Science, Nankai University, Tianjin 300071, China, ⁴School of Mathematics, Shandong University, Jinan 250100, China, ⁵The BioEnergy Science Center, USA and ⁶College of Computer Science and Technology, Jilin University, Changchun, Jilin 130012, China

Received December 6, 2012; Revised March 20, 2013; Accepted March 21, 2013

ABSTRACT

The circular chromosome of *Escherichia coli* has been suggested to fold into a collection of sequentially consecutive domains, genes in each of which tend to be co-expressed. It has also been suggested that such domains, forming a partition of the genome, are dynamic with respect to the physiological conditions. However, little is known about which DNA segments of the *E. coli* genome form these domains and what determines the boundaries of these domain segments. We present a computational model here to partition the circular genome into consecutive segments, theoretically suggestive of the physically folded supercoiled domains, along with a method for predicting such domains under specified conditions. Our model is based on a hypothesis that the genome of *E. coli* is partitioned into a set of folding domains so that the total number of unfoldings of these domains in the folded chromosome is minimized, where a domain is unfolded when a biological pathway, consisting of genes encoded in this DNA segment, is being activated transcriptionally. Based on this hypothesis, we have predicted seven distinct sets of such domains along the *E. coli* genome for seven physiological conditions, namely exponential growth, stationary growth, anaerobiosis, heat shock, oxidative

stress, nitrogen limitation and SOS responses. These predicted folding domains are highly stable statistically and are generally consistent with the experimental data of DNA binding sites of the nucleoid-associated proteins that assist the folding of these domains, as well as genome-scale protein occupancy profiles, hence supporting our proposed model. Our study established for the first time a strong link between a folded *E. coli* chromosomal structure and the encoded biological pathways and their activation frequencies.

INTRODUCTION

It was discovered in 1970s that the *Escherichia coli* chromosome is organized into a collection of consecutive plectonemic DNA loops, each having its two ends connected with each other by binding with nucleoid-associated proteins (NAPs) (1,2). Each of such loops, also called a ‘supercoiled domain’ or simply ‘supercoil’, ranges between 10 and 100 kb in sequence length (3) and folds independent of the other loops into a negatively coiled conformation. It has been speculated that the folded chromosomal structure is dynamic (4), and the domain boundaries are distributed along the genome in a seemingly random manner (5). Imaging data have revealed that the folded conformation of the *E. coli* chromosome changes in response to the changing cellular and environmental conditions (6). For instance,

*To whom correspondence should be addressed. Tel: +1 706 542 9779; Fax: +1 706 542 9751; Email: xyn@bmb.uga.edu

The authors wish it to be known that, in their opinion, the first two authors should be regarded as joint First Authors.

© The Author(s) 2013. Published by Oxford University Press.

This is an Open Access article distributed under the terms of the Creative Commons Attribution Non-Commercial License (<http://creativecommons.org/licenses/by-nc/3.0/>), which permits non-commercial re-use, distribution, and reproduction in any medium, provided the original work is properly cited. For commercial re-use, please contact journals.permissions@oup.com

the chromosome has substantially more supercoils during the exponential growth than during the stationary phase, suggesting that the physical organization of the chromosome may play a role in the regulation of gene expression (7,8). Interestingly, some of the NAPs, which can bend or bridge DNAs, are also transcription factors such as H-NS, FIS and IHF, providing further evidence about the possible links between chromosomal folding and transcription regulation.

The advent and maturation of various experimental techniques such as ‘CHIP-sequencing’ (9–12) techniques for identification of the DNA-binding sites of NAPs and the ‘chromatin conformation capture’ techniques (13–15) have clearly accelerated the study of the folded chromosomal structures, but mostly of eukaryotic organisms. As of now, only limited data on the folded *E. coli* chromosomal structures have been collected mostly focused on the binding of NAPs on the DNA. One recent study on bacterial chromosomes using high-resolution microscope revealed that H-NSs may play a more important role in bacterial chromosomal organization than the other NAPs (16).

A number of computational studies have also been carried out with the goal of understanding the folded structures of bacterial chromosomes. For instance, analyses of *E. coli* ‘omic’ data have revealed periodicities along the genome of co-expressed genes (4,17), as well as of co-evolved genes (18) and *cis*-regulatory elements (19,20), all seemingly related to the supercoils in the folded chromosomal structure. A model for the local arrangement of the *E. coli* chromosomal loci has been proposed based mostly on the geometric consideration (21). In addition, studies have been carried out aiming to capture the relationship among the loop domains based on a confinement and entropic repulsion model as well as the information about transcription regulation networks (22). While these studies have provided hints about possible links between sequence level signals and the folded chromosomal structures, none of them have established a clear definition of the individual folding domains with detailed boundary information, not to mention their dynamic nature with respect to different physiological conditions.

We have recently discovered that operons of more frequently activated pathways tend to group into fewer sequential clusters in a bacterial genome (23), and specifically they tend to minimize the overall genomic spread among the consecutive operons of the same metabolic and regulatory pathway (24,25) across all the pathways. One possible explanation of this discovery is that the *E. coli* chromosome is organized into consecutive domains that minimize the total number of the unfolding of these domains during the life cycle of the organism, where such a domain is unfolded when a biological pathway, consisting of genes encoded in this DNA segment, is being activated transcriptionally; here we use the total number of unfolding to approximate the total energy needed to unfold the relevant folded domains. This hypothesis has been strongly supported by our recent study of the global genomic arrangement of bacterial operons (23). Based on this hypothesis, we have predicted seven distinct sets of folding domains of the *E. coli*

genome under seven different physiological conditions: exponential growth, stationary phase, anaerobiosis, heat shock, oxidative stress, nitrogen limitation and SOS responses. We found that (i) the predicted sets of folding domains are highly stable with respect to perturbations to the gene-expression data used to make the prediction; (ii) they are generally consistent with the limited experimental data on the folded supercoil structures collected under the exponential and stationary growth conditions; and (iii) their boundaries are consistent with the available NAP-binding sites and genome-scale protein occupancy data, hence supporting our prediction. We believe that this study provides an effective framework for elucidation of the chromosomal organization, its dynamic nature and its functional relationship to transcription regulation of *E. coli* and other bacteria.

MATERIALS AND METHODS

Data acquisition

We retrieved the genes encoding the 347 metabolic pathways of *E. coli* K12 from EcoCyc (26), and the expression data from the M3D database (27), which contain genome-scale expression data of *E. coli* collected under 466 conditions. In all, 527 *cis*-regulatory binding sites of six NAPs (Fis, H-NS, HU, IHF, Lrp and StpA) in the *E. coli* genome were downloaded from RegulonDB (28), and 537 binding regions of H-NS under stationary growth conditions are downloaded from (9). In addition, 253 highly expressed genes were obtained from HEG-DB (29), and 272 extensive protein occupancy domains (EPODs) of the *E. coli* genome are downloaded from (30).

Identification of the M3D growth condition groups associated with different folded structures of the chromosome

Based on the knowledge that the *E. coli* chromosome folds into different conformations during the exponential and stationary growths, we expect that under some other growth conditions, the chromosome may fold into alternate conformations to facilitate the efficient activation of the genes for pathways required for each such class of growth conditions. For each folded structure engendered under certain growth conditions, we anticipate that there should be a set of gene responses consistent across these conditions. We call each such class of conditions as a M3D growth condition (MGC) group, and this set of genes as its ‘marker genes’. The determination of each set of marker genes is made based on literature research (31–38) and our understanding of different growth conditions (see Supplementary Method S1). The detailed gene list for each of the seven conditions is given in Supplementary Table S1.

We have used the following procedure to identify the MGC group for each growth condition, collectively denoted as C , along with the associated gene-expression data in M3D. Let G denote the entire gene set of *E. coli* and $G_q \subset G$ be a list of specified marker genes whose activations we suspect should require a distinct folded structure of the chromosome, with $|G|$ and $|G_q|$

representing the number of genes in G and G_q , respectively. Also let $A = \{a_{ij}\}_{|G| \times |C|}$ denote the whole M3D dataset, with a_{ij} representing the expression value of gene i under condition j and $|C|$ representing the number of conditions in the M3D dataset, and $A' = \{a'_{ij}\}_{m \times n}$ be a 0/1 matrix, with a'_{ij} being 1 if a_{ij} is among the highest (or the lowest depending on specific applications) 25% of the values in $\{a_{i1}, a_{i2}, \dots, a_{in}\}$, otherwise 0, where $\{a_{i1}, a_{i2}, \dots, a_{in}\}$ is the i^{th} row of matrix A , i.e. the expression levels of gene i under all the conditions. Our goal is to identify MGCs as maximal subsets of C under which the majority of the marker genes in each G_q are highly expressed, i.e. their corresponding values in A' being 1. Specifically, we define

$$MGC_q = \left\{ j \mid \frac{\sum_{i \in G_q} a'_{ij}}{|G_q|} \in [0.8, 1], 1 \leq j \leq n \right\}$$

for each given G_q . In case an MGC_q is empty, we will go back to adjust the threshold in $[0.8, 1]$ so each MGC_q is a non-empty set.

Prediction of the folding domains for each MGC group

Our main hypothesis (see ‘Introduction’ section) implies that (i) the genome of *E. coli* is partitioned into a set of contiguous domains, each independently folded into a compact structure in the folded chromosome; and (ii) under different growth conditions, the chromosome forms different sets of such folding domains, where the domain regions are so determined that minimizes the total number of unfolding of the folded domains to make their genes transcriptionally accessible when needed. Based on these, we have made a computational prediction of the domain boundaries along the genome by formulating the problem as a constrained optimization problem below.

Based on the published literature, we assume that the folding domains range $L = 10$ kb and $U = 100$ kb in length (3), and the domain boundaries can be only in inter-operonic regions. So our problem formulation is to find a partition of the *E. coli* K12 circular genome so that the following objective function is minimized:

$$OF_{\text{pathway}} = OF_1 + \alpha OF_2 \quad (1)$$

with

$$OF_1 = \sum_{i=1}^N f_i t_i \quad (2)$$

and

$$OF_2 = \sum_{i=1}^N f_i \sum_{j=1}^M \omega_{ij} \quad (3)$$

where M is the number of to-be-identified folding domains; OF_1 is the number of unfolding of the predicted domains to make the relevant pathways transcriptionally accessible (we assume that each domain will refold after the transcription of its relevant genes is all done so the unfolding is needed again when its genes need to be transcribed later); N is the number of known metabolic

pathways encoded in the organism; f_i represents the activation frequency of the i^{th} pathway, estimated from the gene expression data in M3D using the method given in (24); t_i is the number of predicted folding domains that have genes encoding the i^{th} pathway and OF_2 approximates the unfolding energy ‘wasted’ on unfolding the folded domains under the current condition (here we assume that (i) the effort (or energy) in unfolding a folding domain is proportional to the number of operons it contains; and (ii) the energy wasted is proportional to the number of operons contained in the domain but not involved in the pathway being activated under the current condition). For the j^{th} domain ($j \in [1, M]$) containing s_j operons, s_{ij} is the number of operons in the j^{th} domain and in the i^{th} pathway; $\omega_{ij} = 0$ if $s_{ij} = 0$, otherwise $\omega_{ij} = s_j - s_{ij}$; α is a scaling factor whose value can be adjusted with its default value set at 1.

We noted that the pathway information alone does not constrain the domain prediction problem to a satisfactory level, making the problem a highly under-constrained optimization problem with a large number of solutions; hence, we included co-expression data as an additional constraint to further constrain the prediction problem. Intuitively we expect that genes in the same folding domain should be co-expressed more frequently than genes not in the same domain. We therefore developed the following objective term $OF_{\text{expression}}$ over domain boundaries (x_j, y_j) , with x_j and y_j being two adjacent genes separated by an inter-operonic region, representing the last and the first gene of the to-be-identified j^{th} and $(j+1)^{\text{th}}$ folding domains under the current growth condition, respectively:

$$OF_{\text{expression}} = \sum_{j=1}^M L(x_j, y_j) \quad (4)$$

where $L(\cdot)$ is designed to measure the overall co-expression level among gene pairs across each domain boundary (x_j, y_j) , which can be determined as to find a set of M gene pairs (x_j, y_j) as potential domain boundaries so $\sum_{j=1}^M L(x_j, y_j)$ is minimized,

$$L(x, y) = \sum_{\substack{(X, Y) \text{ are coexpressed} \\ d_X \leq d_x, d_Y \geq d_y \\ d_Y - d_X \leq 20K}} \left(\frac{n_{X, Y} \times S(p_X, p_Y)}{\sqrt{(d_x - d_X + 1) \times (d_Y - d_Y + 1)}} \right) \quad (5)$$

where $M > 0$ is to be determined through solving this minimization problem; d_x represents the genomic location of gene x ; (X, Y) denotes all the gene pairs across the inter-genic region between genes x and y with distance ≤ 20 kb; p_X and p_Y are vectors of expression levels of X and Y under the current growth condition; $n_{X, Y}$ is the number of MGCs under which X and Y are co-expressed; and $S(\cdot)$ is the Spearman rank correlation coefficient (39).

Now our enhanced formulation of the domain identification problem is defined as ‘to find a partition of the given circular genome to minimize the following’

$$AOF(S, E) = OF_1 + \alpha OF_2 + \beta OF_{\text{expression}} \quad (6)$$

where S and E represent the first and the last inter-operonic regions of the genome, respectively.

This optimization problem can be solved using a dynamic programming approach. Specifically, we have the following recursive relationship, which can be proved without a substantial effort:

$$AOF(S, i) = \min_{j \in [i-U, i-L]} [AOF(S, j) + AOF(j, i)] \quad (7)$$

which gives rise to a straightforward dynamic programming algorithm for solving this optimization problem, and further gives rise to the predicted domain boundaries under the specified growth conditions.

Measuring distance between two sets of predicted folding domains

To assess the prediction performance of the above algorithm, we need a capability to estimate the distance between two different sets of predicted folding domains (i.e. the distance between two different genomic partitions). Consider two sets of predicted domain boundaries (each represented as a set of inter-operonic regions), B_1 and B_2 , of the same (circular) genome. Let $I = B_1 \cap B_2$ and $U = B_1 \cup B_2$ represent the intersection and union of B_1 and B_2 , respectively. Note that the distance between B_1 and B_2 should be 0 if I and U are identical. The larger the difference between I and U is, the larger the distance between B_1 and B_2 should be. In defining the distance, we consider that the distance between B_1 and B_2 is larger when boundaries in $U - I$ are more spread out across the genome when $|U - I|$ is fixed. Let $\{x_i\}_{1 \leq i \leq |I|}$ and $\{y_j\}_{1 \leq j \leq |U|}$ denote the sets of predicted boundaries of I and U , respectively, ordered clockwise along the circular genome starting at the origin of replication, and $x_0(y_0)$ and $x_{|I|+1}(y_{|U|+1})$ be the origin of replication. For any two consecutive boundaries in I , x_i and x_{i+1} , the number of boundaries in $U - I$ between x_i and x_{i+1} is denoted as $d(x_i, x_{i+1})$ so the average value is $\mu = \frac{\sum_{i=0}^{|I|} d(x_i, x_{i+1})}{|I|+1} = \frac{|U-I|}{|I|+1}$. Clearly the larger the $|x_i = \arg\{d(x_i, x_{i+1}) \geq \mu\}|$ value is, the more spread out across the genome the boundaries in $U - I$ are. We define the distance between B_1 and B_2 as

$$S = \left(1 - \frac{|I|}{|U|}\right) \times \frac{|x_i = \arg\{d(x_i, x_{i+1}) \geq \mu\}|}{|I|} \quad (i = 0, 1, \dots, |I|) \quad (8)$$

We can see that the more similar two genomic partitions are, the smaller the distance will be.

RESULTS

Generation of MGC groups

Knowing that the *E. coli* chromosome folds into different structures during exponential growth and stationary growth (1), we identified the subset of the 466 growth conditions in M3D associated with each of these two growth phases. Specifically, we used the expression levels

Table 1. Information of the seven classes of growth conditions with the marker genes used for identifying the growth condition classes in M3D listed in the second column (with the gene number following in the brackets) and the number of MGC sets for each growth condition class shown in the third column

Growth conditions	Marker genes (number of genes)	Number of MGC datasets
Exponential growth	Ribosomal proteins (54)	45
Stationary growth	Ribosomal proteins (54)	131
Heat shock	Heat shock proteins (14)	54
Oxidative stress	OxyR and SoxRS regulons (61)	30
Anaerobiosis	Partial Fnr regulons (53)	55
SOS response	LexA regulon (56)	57
Nitrogen limitation	NtrC and Nac regulon (65)	34
Random	N/A	100

The 'Random' growth conditions (the last line in Table 1) correspond to 100 randomly selected MGCs from all the available MGC in the M3D database.

of 54 ribosomal protein genes to define the two corresponding MGC groups: conditions under which most of these ribosomal proteins are highly expressed and conditions under which ribosomal proteins are overall lowly expressed, respectively (see 'Materials and Methods' section). These two MGC sets are referred to as two groups of growth conditions. We further hypothesize that other classes of growth conditions may also give rise to distinctly folded chromosomal structures. Specifically, we have considered the following five widely studied classes of growth conditions associated with anaerobiosis, oxidative stress, heat shock, nitrogen limitation and SOS response, and derived corresponding MGCs for each of them using marker genes known to be upregulated under each such condition (31–38). Table 1 lists the marker genes for each of these seven classes of growth conditions along with the associated information (for more details, see Supplementary Tables S1 and S2). Overall, seven MGC groups are identified covering 325 out of the 466 growth conditions in M3D, for each of which we made the prediction of the folding domain boundaries of the *E. coli* genome.

Prediction of folding domains of *E. coli* under a specified class of growth conditions

We predicted the folding-domain boundaries of the *E. coli* genome under each of the seven classes of growth conditions shown in Table 2. One hundred forty-six folding domains are predicted for the exponential growth, 84 for the stationary growth, 116 for heat shock, 95 for nitrogen limitation, 94 for oxidative stress, 102 for anaerobiosis and 114 for SOS response. Figure 1a shows the predicted domains under stationary growth along the *E. coli* K12 genome. Figure 1b is an expanded view of the genomic region (0–1.2 M) in Figure 1a. From Figure 1b, we can see that the predicted folding domains indeed show higher levels of co-expression than gene pairs across the domain boundaries as desired, with the detailed data shown in Figure 1c. An example of

Table 2. Properties of the folding-domain boundaries predicted for each MGC group

MGC groups	Number of folding-domain boundaries	ALD (kb)	ALB (bp)	ALNB (bp)	#HEG	#NAP	#Transcription factories	#Fis
Exponential growth	146	31.4	402	271	13	43	6	33
Stationary growth	84	54.9	351	276	10	24	3	16
Heat shock	116	39.6	424	193	13	31	6	19
Oxidative stress	94	48.9	344	276	3	31	2	15
Anaerobiosis	102	45	424	272	13	33	8	21
SOS response	114	40.2	471	269	6	34	1	20
Nitrogen limitation	95	48.5	344	276	4	26	1	18

ALD, average length of the predicted folding domains; ALB, average length of the inter-operonic regions containing folding-domain boundaries; ALNB, average length of the remaining inter-operonic regions. #HEG is the number of highly expressed genes encoded in the predicted folding-domain boundary regions. #NAP is the number of NAP binding sites in the inter-operonic regions containing a predicted folding-domain boundary. #Transcription factories is the number of superstructures near predicted folding-domain boundaries formed by NAPs associated with the ribosomal RNA operons. #Fis is for the number of Fis binding sites in the inter-operonic regions containing a predicted folding-domain boundary.

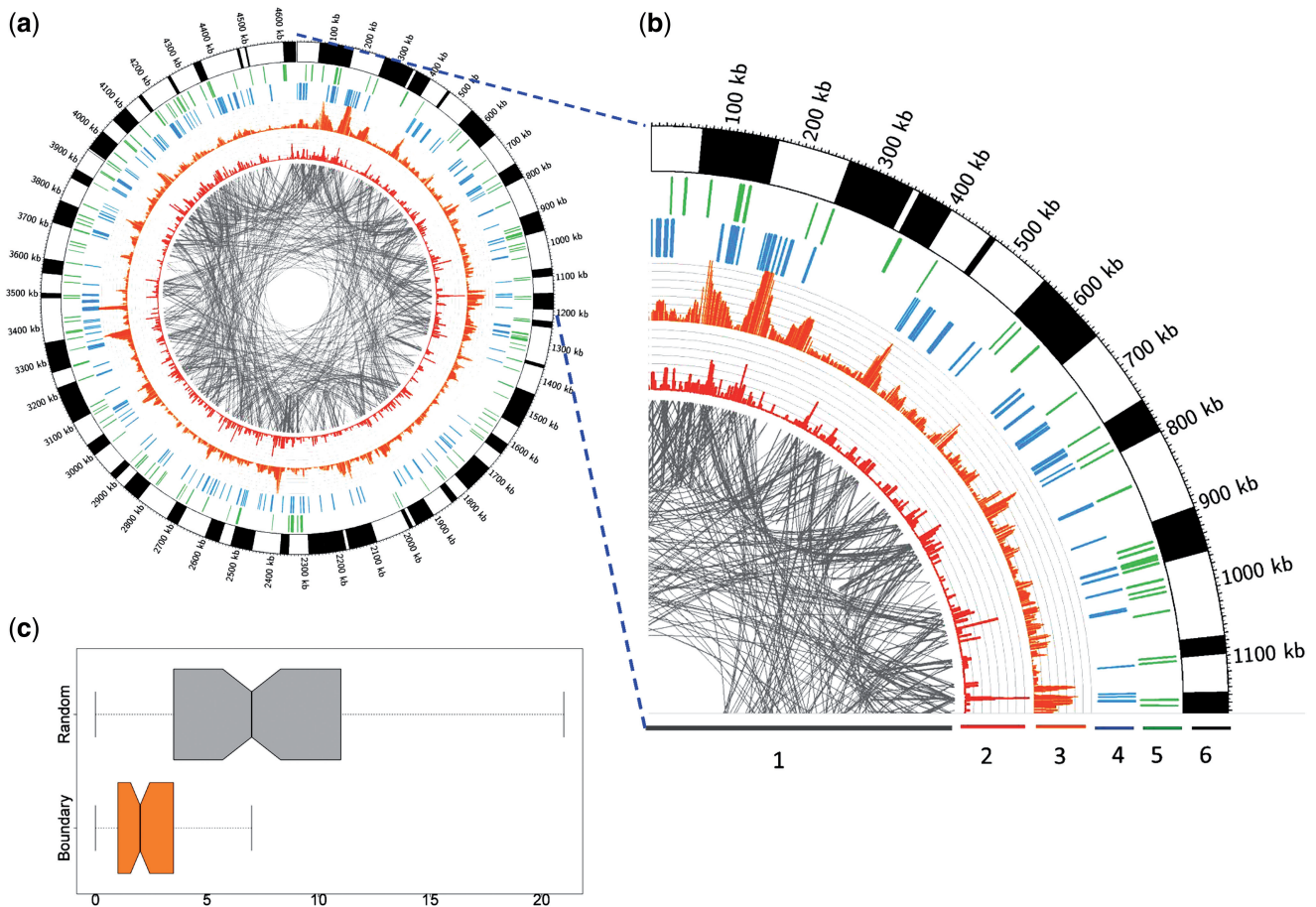


Figure 1. (a) Circos plots of predicted folding domains along the genome of *E. coli* K12 during the stationary growth phase. The alternating black and white bands in the outermost ring represent the partition of the *E. coli* genome into folding domains. (b) An expanded view of the genomic region (0–1.2 M). From the inside out, the six rings are labeled with numbers: (1) Each pair of genes involved in the same EcoCyc pathway are connected using gray lines; (2) the red histogram shows the number of pathways in which the target gene is involved; (3) the orange histogram shows the number of the coexpressed gene pairs; (4) each blue bar represents the presence of a highly expressed gene; (5) each green bar represents the presence of a known NAP-binding site, which should fall in domain boundary regions; and (6) predicted folding domains represented as alternating black-and-white bands in the seventh ring. Two thick bars are used to distinguish the adjacent folding domains as the boundaries are not visible at genome scale. (c) A comparison between the numbers of coexpressed gene pairs in the flanks of the predicted domains (orange box) and a set of randomly picked intergenic regions (gray box).

the predicted domains and associated co-expression data can be found in Supplementary Example S1 and Supplementary Table S3.

Overall, 409 out of 2367 inter-operonic regions in the *E. coli* genome (40) serve as a boundary of at least one predicted domain (*B*), while the remaining 1958 do not (*NB*). We also noted that 45.3% of the predicted boundaries are shared by at least two MGC groups and 23.5% by at least three MGC groups. The detailed boundary information of the predicted domains, along with other related information is given in Supplementary Table S4.

Stability of the predicted folding-domain boundaries

As there are no large-scale experimental data collected on the folded *E. coli* chromosomal structures to validate our prediction, we have to assess the reliability of the predicted folding domains mostly computationally. Specifically, we have assessed the stability of each predicted set of domains by perturbing the gene expression dataset used to make the prediction. The approach was to replace a fraction of the used MGC set by the same number of unrelated conditions randomly selected from the remaining growth conditions out of the 466 in M3D. We would expect that a correctly predicted set of folding domains should be highly consistent and reproducible, whereas randomly or incorrectly predicted domains should not.

We used the following procedure, along with the distance measure defined in 'Materials and Methods' section, to assess the prediction stability. Let *C* be the condition set used to predict a set of folding domains. We randomly selected 50% of the conditions from *C*, denoted it as *S1* and let *S2* contain 25% of conditions randomly selected from *C* and the same number of conditions randomly selected from the remaining portion of the 466 conditions after removing *C*. We then predicted the set of folding domains under conditions *C*, *S1* and *S2*, denoting the three sets of predicted domains as *P*, *P1* and

P2, respectively. We performed such predictions 1000 times for each *C* corresponding each condition class given in Table 2 and calculated the distance distributions between *P* and *P1* and between *P* and *P2*. Figure 2 shows the box plots of the two distributions for each of the seven classes of conditions, plus a randomly selected condition set *C* out of 466, with the same number of conditions to that of the above. We can clearly see that the distance between *P* and *P1* is significantly smaller than that between *P* and *P2* (all achieving Wilcoxon test $P < 2.2e-9$, shown in Figure 2) for all the seven condition sets, and there is virtually no difference for the random set. Hence, we can conclude that each predicted folding-domain set based on any of the seven classes of conditions is highly statistically significant compared with domains predicted based on randomly selected conditions, hence suggesting the strong biological significance of the predicted domains.

Functional inference of genes located close to the predicted folding-domain boundaries

We have examined the predicted domains to check if genes located close to the domain boundaries may have distinct characteristics compared with other genes. We noted that such genes tend to have higher GC content and higher expression levels than the other genes. Specifically, we have calculated the *P*-value of the Wilcoxon test with the null hypothesis that such genes having no higher GC content and expression values than the other genes, which gives rise to $P < 0.05$ for the test. See Supplementary Figure S1 for the detailed information. Interestingly, previous studies have shown that there is a positive correlation between the expression value and GC content (41), providing an indirect evidence supporting our observation.

We have also performed a gene ontology 'biological process' (42) enrichment analysis on genes flanking the predicted folding-domain boundaries using DAVID (43).

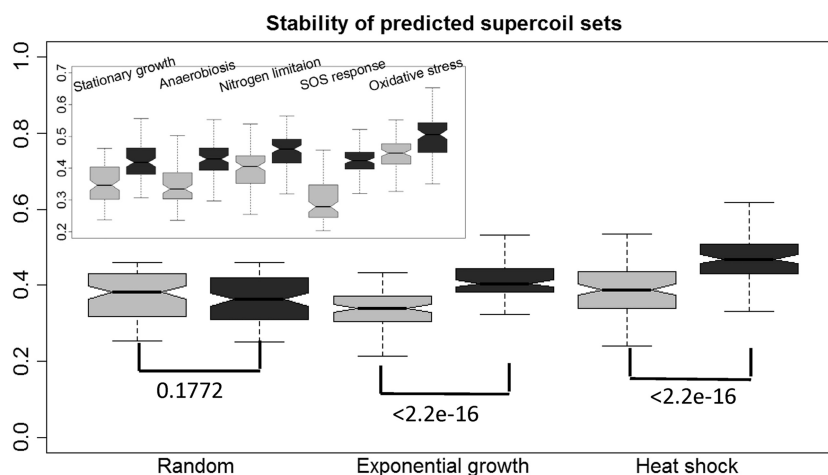


Figure 2. Boxplots showing stabilities of the predicted folding domains (exponential growth and heat shock) based on the selected MGC set versus a randomly selected MGC set as defined in the main text. The comparison among the other five pairs of predicted domain sets is shown in the left upper corner. Each box with lighter gray level represents the distance distribution between the domains predicted using the selected MGCs and domains predicted using half of the selected MGCs, and each box with darker gray level is defined similarly but against domains predicted based on randomly selected MGCs, where the *y*-axis is the distance axis. The Wilcoxon test *P*-values for each pair of distributions are shown in the top of boxes of each corresponding set of predicted folding domains.

Our result indicates that some genes involved in nitrogen and sulfur metabolisms are enriched for five of the seven classes of conditions (except for anaerobiosis and oxidative stress). For instance, 76 out of the 494 genes flanking the domain boundaries during the exponential growth are involved in nitrogen, purine and amino acid metabolisms. In particular, this set of genes contains those encoding biosynthesis pathways of spermidine from glutamate, arginine degradation, nitrogen and sulfur assimilation, as well as proline and purine biosynthesis. The enrichment of these genes suggests that these genes are actively transcribed, which is consistent with our observation

made in Supplementary Figure S1b that genes flanking the domain boundaries tend to express at higher levels than the other genes.

Comparisons among the seven sets of predicted domains

We have compared the seven sets of predicted folding domains based on seven sets of distinct MGCs defined earlier, using the following two measures: (i) the degree of overlap in growth conditions between two different MGC groups, and (ii) the distance between each pair of predicted domain sets. The ‘degree of overlap’ is defined as $\frac{|A \cap B|}{|A \cup B|}$, where A and B represent two MGC groups.

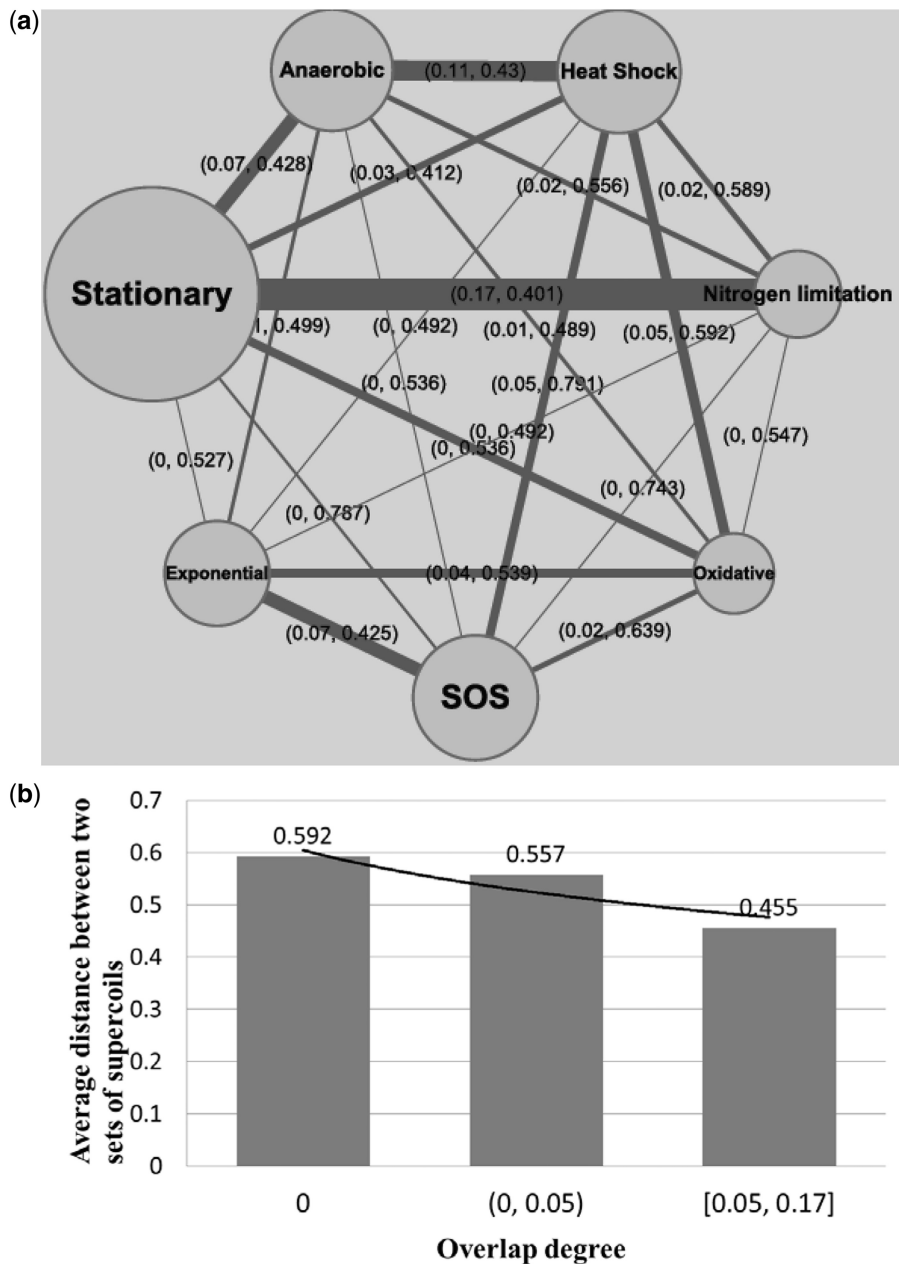


Figure 3. (a) Degrees of overlap between each pair of MGC groups. The node size represents the size of a MGC group, and the edge width represents the number of overlapping MGCs between the two corresponding nodes. The label of each edge has two values: the first being the degree of overlap between the two corresponding MGC groups and the second being the distance between two predicted folding-domain sets, and (b) relationship between the degree of overlap among MGC groups and the distance between the corresponding folding-domain sets.

First, we noted that >90% (19 out of $C_2^7 = 21$) of the MGC group pairs have the degree of overlap scores <0.1, indicating that the seven classes of MGCs are largely independent of each other. As expected, a higher level of overlaps between two classes of MGCs tends to give rise to smaller distances between their predicted folding-domain sets, as shown in Figure 3b. For instance, the two classes of MGCs, stationary growth and nitrogen limitation, have the highest degree of overlap at 0.17 as shown in Figure 3a and also have the smallest distance, 0.401, between their predicted folding-domain sets among all the pairwise comparisons. This is not unexpected because in stationary phase, cells stop multiplying exponentially in part owing to limitation of some essential nutrients. Another two sets of domains with a small distance, 0.43, are under anaerobiosis and heat shock. Their corresponding MGC groups have the second largest degree of overlap 0.11. There are no overlapping MGCs between the classes of stationary growth and SOS response at all, and they have a relatively large distance at 0.787.

Comparison between domain boundaries and experimental data

Using an *in vivo* protein occupancy experiment, 272 EPODs of the *E. coli* chromosome have been identified in (30). The EPODs are enriched with NAP-binding sites (see details in Supplementary Table S5) and play an important role in the folding of the *E. coli* chromosome. These domains can be grouped into two classes: the transcriptionally silent class (tsEPODs) and the highly expressed class (heEPODs). The 151 tsEPODs are located across the genome apparently randomly and has proved to have bigger influence on the organizational architecture of the folded *E. coli* chromosome than the heEPODs (30), totaling 121. In addition, we have also retrieved 537 H-NS binding regions under the stationary growth condition from (9), knowing that H-NSs play a key role in the formation of supercoil structures in the folded *E. coli* chromosome (16). These H-NS binding regions can be classified to long H-NS (loH-NSs) and short H-NS binding regions (shH-NSs), with the longer H-NSs wrapping around larger segments of the *E. coli* chromosome. We have compared the predicted folding-domain boundaries under the stationary growth condition [stationary folding domains (sFDs)] with these EPODs and H-NS binding regions as follows.

Let A denote all the inter-operonic regions in *E. coli* genome, and B be the subset of A that has been computationally predicted by our algorithm; C denotes the subset of A , which is experimentally identified. We use the following P -value calculation to assess the statistical significance of the level of coincidence between B and C . Specifically, if our prediction B is random, then the probability of B and C sharing exactly m inter-operonic regions is

$$p_A(m|B, C) = \frac{\binom{|C|}{m} \binom{|A| - |C|}{|B| - m}}{\binom{|A|}{|B|}}$$

Table 3. Statistical significance of correlation coefficient between predicted domain boundaries and EPODs and H-NS binding regions

	EPODs	tsEPODs	heEPODs	H-NSs	loH-NSs	shH-NSs
sFDs	3.8e-03*	2.6e-02*	6.4e-02	1.1e-02*	4.1e-02*	8.3e-02
Random set	4.2e-01	2.3e-01	6.1e-01	9.7e-02	9.2e-02	5.4e-01

* $P < 0.05$.

where $|X|$ denotes the number of elements in X and $m = |B \cap C|$. Hence, the P -value in respect to the assumption is $p_A(x \geq m|B, C)$, denoted as $P_A(B, C)$.

We note that the P -values $P_A(sFDs, EPODs)$ and $P_A(sFDs, tsEPODs)$ are both <0.05, but $P_A(sFDs, heEPODs)$ is not. Between sFDs and the H-NS binding regions, $P_A(sFDs, H-NSs)$ and $P_A(sFDs, loH-NSs)$ are <0.05 but $P_A(sFDs, shH-NSs)$ is not (see Table 3). These results indicate that our predicted folding domains have substantial overlaps with EPODs and H-NS-binding regions, and they tend to have higher level of overlap with the tsEPODs and loH-NSs, which are known to cast bigger influence on the folded chromosomal structures than heEPODs and shH-NSs. As a comparison, we have randomly picked a set of inter-operonic regions as potential domain boundaries and done the same calculation on sFDs, the P -values are consistently higher than those calculated using predicted domain boundaries as shown in Table 3.

DISCUSSION

Predicted folding domains under exponential and stationary growth conditions are generally consistent with the available experimental data

We have noted from Table 2 that the numbers of folding domains predicted under the exponential growth and the stationary growth conditions are generally consistent with the experimentally observed number of supercoils using electron microscopy (1). Specifically, the data indicate that the folded chromosomal structure has substantially more supercoils during the exponential growth than those during the stationary growth phase, which is consistent with our predicted numbers of folding domains under the two conditions, 146 versus 84. And some Fis-binding sites are exposed more frequently during the exponential growth than during the stationary growth, consistent with our predicted numbers 33 versus 16. In addition, there are more transcription factories operating during the exponential growth than during the stationary growth, consistent with the numbers 6 versus 3 based on our prediction, where a 'transcription factory' is defined as a spatially confined aggregation of RNA polymerase, transcription factors and NAPs in nucleoid (44). The detailed calculation of these numbers based on our predictions is given in Table 2.

Sequence features indicate a strong link between the predicted folding domains and supercoils in the folded chromosome

We have noted that the average length of the inter-operonic regions in *B* is 414 bp, which is significantly longer than the average length of *NB*, 250 bp (see 'Materials and Methods' section). This clearly makes sense as NAPs are expected to bind near the supercoil boundaries and hence require extra space in the binding-site containing inter-operonic regions (detailed comparisons can be found in Supplementary Figure S2). The higher expression levels of genes flanking the folding-domain boundaries (Supplementary Figure S1b) suggest that these genes are more actively transcribed compared with those in the internal portions of the folding domains. Hence, we speculate that the active transcription of genes flanking the boundaries might be accompanied by pushing the coiling toward the center of the supercoiled domains, hence making the middle portions of the supercoils more tightly coiled than the boundary regions, and reducing their accessibility by the RNA polymerases and the transcription levels.

Potential limitations of our predicted MGCs

For each of the seven physiological conditions, its set of marker genes is manually collected from the published studies on the seven conditions. While the seven identified subsets of conditions are biologically meaningful and statistically significant, the marker genes are not selected in a systematic manner and hence could have limited the effectiveness of our method. To examine this issue, we have carried out a *de novo* biclustering (45,46) of the expression data of *E. coli* in M3D and obtained 17 condition clusters with high statistical significance (shown in Supplementary Table S6). Out of these 17 clusters, six have low a degree of overlap with the seven MGC groups (<0.15), indicating that these subsets of conditions, not covered by current seven MGC groups, may correspond to certain physiological conditions that have not been systematically studied, and hence warrants further studies. We plan to carry a detailed and systematic analysis of the 17 biclusters to identify their corresponding physiological conditions as well as their potentially corresponding folded chromosomal structures of *E. coli* K12.

CONCLUDING REMARK

We have predicted a distinct set of folding domains of the *E. coli* K12 chromosome for each of seven sets of growth conditions based on the gene-expression data in M3D, the most comprehensive gene-expression dataset on *E. coli*, along with pathway information from EcoCyc. These predicted domains are highly stable with respect to perturbations to the expression data based on which the prediction is made. They also show good agreement with the available *E. coli* folded chromosomal structure data, including experimental observation and high-throughput NAP-binding regions. The results of the computation and analysis provided strong evidence supporting our main hypothesis that operons encoding *E. coli*

metabolic pathways are arranged along the genome that tends to minimize the total effort, measured using the number of total unfolding of the folded domains, to make the genes of the needed pathways transcriptionally accessible. We believe that this study provides a framework for studying the functional constraints cast on the genomic organization of operons in *E. coli* and bacteria in general. We fully expect that the same study can be applied to other bacterial genomes, for which substantial amounts of gene-expression data collected under multiple conditions are available. Such predicted folding-domain boundaries, when fully validated by and applied in conjunction with the information derived from the emerging chromosome conformation capture techniques, could prove to be essential to understanding the detailed regulation mechanisms of transcription relating to dynamic supercoiling, as well as the general principles that govern the genomic locations of operons (24,25).

The program used to generate the data used in this article was written in ANSI C and tested using GCC (version 4.1.2) on Linux. The source code is available at: <http://code.google.com/p/supercoil/>.

SUPPLEMENTARY DATA

Supplementary Data are available at NAR Online: Supplementary Tables 1–6, Supplementary Figures 1 and 2, Supplementary Method 1, Supplementary Example 1 and Supplementary References [1,3,6–8,13–16,47].

ACKNOWLEDGEMENTS

Y.X. conceived the basic idea and planned the project. Q.M. developed the software and carried out the experiments. Y.Y. and Q.M. analyzed the data and wrote the manuscript. M.S. proposed several good suggestions for the 'Results' section in the view of biology. G.L. designed and polished the algorithm. H.Z. contributed to the gene expression analysis. All authors edited the manuscript and approved the final manuscript.

FUNDING

National Science Foundation (#NSF DEB-0830024 and NSF MCB-0958172) (in part); the US Department of Energy's BioEnergy Science Center (BESC) grant through the Office of Biological and Environmental Research. The BioEnergy Science Center is a U.S. Department of Energy Bioenergy Research Center supported by the Office of Biological and Environmental Research in the DOE Office of Science. Funding for open access charge: US Department of Energy's BioEnergy Science Center (BESC).

Conflict of interest statement. None declared.

REFERENCES

1. Dillon, S.C. and Dorman, C.J. (2010) Bacterial nucleoid-associated proteins, nucleoid structure and gene expression. *Nat. Rev. Microbiol.*, **8**, 185–195.

2. Benza, V.G., Bassetti, B., Dorfman, K.D., Scolari, V.F., Bromek, K., Cicuta, P. and Lagomarsino, M.C. (2012) Physical descriptions of the bacterial nucleoid at large scales, and their biological implications. *Rep. Prog. Phys.*, **75**, 076602.
3. Noom, M.C., Navarre, W.W., Oshima, T., Wuite, G.J. and Dame, R.T. (2007) H-NS promotes looped domain formation in the bacterial chromosome. *Curr. Biol.*, **17**, R913–R914.
4. Postow, L., Hardy, C.D., Arsuaga, J. and Cozzarelli, N.R. (2004) Topological domain structure of the *Escherichia coli* chromosome. *Genes Dev.*, **18**, 1766–1779.
5. Luijsterburg, M.S., Noom, M.C., Wuite, G.J. and Dame, R.T. (2006) The architectural role of nucleoid-associated proteins in the organization of bacterial chromatin: a molecular perspective. *J. Struct. Biol.*, **156**, 262–272.
6. Stein, R.A., Deng, S. and Higgins, N.P. (2005) Measuring chromosome dynamics on different time scales using resolvases with varying half-lives. *Mol. Microbiol.*, **56**, 1049–1061.
7. Rocha, E.P. (2008) The organization of the bacterial genome. *Annu. Rev. Genet.*, **42**, 211–233.
8. Browning, D.F., Grainger, D.C. and Busby, S.J. (2010) Effects of nucleoid-associated proteins on bacterial chromosome structure and gene expression. *Curr. Opin. Microbiol.*, **13**, 773–780.
9. Kahramanoglou, C., Seshasayee, A.S., Prieto, A.I., Ibberson, D., Schmidt, S., Zimmermann, J., Benes, V., Fraser, G.M. and Luscombe, N.M. (2011) Direct and indirect effects of H-NS and Fis on global gene expression control in *Escherichia coli*. *Nucleic Acids Res.*, **39**, 2073–2091.
10. Grainger, D.C., Aiba, H., Hurd, D., Browning, D.F. and Busby, S.J. (2007) Transcription factor distribution in *Escherichia coli*: studies with FNR protein. *Nucleic Acids Res.*, **35**, 269–278.
11. Grainger, D.C., Hurd, D., Goldberg, M.D. and Busby, S.J. (2006) Association of nucleoid proteins with coding and non-coding segments of the *Escherichia coli* genome. *Nucleic Acids Res.*, **34**, 4642–4652.
12. Prieto, A.I., Kahramanoglou, C., Ali, R.M., Fraser, G.M., Seshasayee, A.S. and Luscombe, N.M. (2012) Genomic analysis of DNA binding and gene regulation by homologous nucleoid-associated proteins IHF and HU in *Escherichia coli* K12. *Nucleic Acids Res.*, **40**, 3524–3537.
13. Simonis, M., Klous, P., Splinter, E., Moshkin, Y., Willemsen, R., de Wit, E., van Steensel, B. and de Laat, W. (2006) Nuclear organization of active and inactive chromatin domains uncovered by chromosome conformation capture-on-chip (4C). *Nat. Genet.*, **38**, 1348–1354.
14. Dekker, J., Rippe, K., Dekker, M. and Kleckner, N. (2002) Capturing chromosome conformation. *Science*, **295**, 1306–1311.
15. Zhao, Z., Tavoosidana, G., Sjolinder, M., Gondor, A., Mariano, P., Wang, S., Kanduri, C., Lezcano, M., Sandhu, K.S., Singh, U. *et al.* (2006) Circular chromosome conformation capture (4C) uncovers extensive networks of epigenetically regulated intra- and interchromosomal interactions. *Nat. Genet.*, **38**, 1341–1347.
16. Wang, W., Li, G.W., Chen, C., Xie, X.S. and Zhuang, X. (2011) Chromosome organization by a nucleoid-associated protein in live bacteria. *Science*, **333**, 1445–1449.
17. Deng, S., Stein, R.A. and Higgins, N.P. (2005) Organization of supercoil domains and their reorganization by transcription. *Mol. Microbiol.*, **57**, 1511–1521.
18. Wright, M.A., Kharchenko, P., Church, G.M. and Segre, D. (2007) Chromosomal periodicity of evolutionarily conserved gene pairs. *Proc. Natl Acad. Sci. USA*, **104**, 10559–10564.
19. Kepes, F. (2004) Periodic transcriptional organization of the *E. coli* genome. *J. Mol. Biol.*, **340**, 957–964.
20. Jeong, K.S., Ahn, J. and Khodursky, A.B. (2004) Spatial patterns of transcriptional activity in the chromosome of *Escherichia coli*. *Genome Biol.*, **5**, R86.
21. Buenemann, M. and Lenz, P. (2011) Geometrical ordering of DNA in bacteria. *Commun. Integr. Biol.*, **4**, 291–293.
22. Fritsche, M., Li, S., Heermann, D.W. and Wiggins, P.A. (2012) A model for *Escherichia coli* chromosome packaging supports transcription factor-induced DNA domain formation. *Nucleic Acids Res.*, **40**, 972–980.
23. Ma, Q. and Ying, X. (2013) Global genomic arrangement of bacterial genes is closely tied with the total transcriptional efficiency. *Genomics Proteomics Bioinformatics*, **11**, 66–71.
24. Yin, Y., Zhang, H., Olman, V. and Xu, Y. (2010) Genomic arrangement of bacterial operons is constrained by biological pathways encoded in the genome. *Proc. Natl Acad. Sci. USA*, **107**, 6310–6315.
25. Zhang, H., Yin, Y., Olman, V. and Xu, Y. (2012) Genomic arrangement of regulons in bacterial genomes. *PLoS One*, **7**, e29496.
26. Karp, P.D., Riley, M., Saier, M., Paulsen, I.T., Collado-Vides, J., Paley, S.M., Pellegrini-Toole, A., Bonavides, C. and Gama-Castro, S. (2002) The EcoCyc Database. *Nucleic Acids Res.*, **30**, 56–58.
27. Faith, J.J., Driscoll, M.E., Fusaro, V.A., Cosgrove, E.J., Hayete, B., Juhn, F.S., Schneider, S.J. and Gardner, T.S. (2008) Many Microbe Microarrays Database: uniformly normalized Affymetrix compendia with structured experimental metadata. *Nucleic Acids Res.*, **36**, D866–D870.
28. Gama-Castro, S., Salgado, H., Peralta-Gil, M., Santos-Zavaleta, A., Muniz-Rascado, L., Solano-Lira, H., Jimenez-Jacinto, V., Weiss, V., Garcia-Sotelo, J.S., Lopez-Fuentes, A. *et al.* RegulonDB version 7.0: transcriptional regulation of *Escherichia coli* K-12 integrated within genetic sensory response units (Sensor Units). *Nucleic Acids Res.*, **39**, D98–D105.
29. Puigbo, P., Romeu, A. and Garcia-Vallve, S. (2008) HEG-DB: a database of predicted highly expressed genes in prokaryotic complete genomes under translational selection. *Nucleic Acids Res.*, **36**, D524–D527.
30. Vora, T., Hottes, A.K. and Tavaoize, S. (2009) Protein occupancy landscape of a bacterial genome. *Mol. Cell*, **35**, 247–253.
31. Lindquist, S. and Craig, E.A. (1988) The heat-shock proteins. *Annu. Rev. Genet.*, **22**, 631–677.
32. De Maio, A. (1999) Heat shock proteins: facts, thoughts, and dreams. *Shock*, **11**, 1–12.
33. Tolla, D.A. and Savageau, M.A. (2010) Regulation of aerobic-to-anaerobic transitions by the FNR cycle in *Escherichia coli*. *J. Mol. Biol.*, **397**, 893–905.
34. Kang, Y., Weber, K.D., Qiu, Y., Kiley, P.J. and Blattner, F.R. (2005) Genome-wide expression analysis indicates that FNR of *Escherichia coli* K-12 regulates a large number of genes of unknown function. *J. Bacteriol.*, **187**, 1135–1160.
35. Cabiscol, E., Tamarit, J. and Ros, J. (2000) Oxidative stress in bacteria and protein damage by reactive oxygen species. *Int. Microbiol.*, **3**, 3–8.
36. Michel, B. (2005) After 30 years of study, the bacterial SOS response still surprises us. *PLoS Biol.*, **3**, e255.
37. Ninfa, A.J., Jiang, P., Atkinson, M.R. and Peliska, J.A. (2000) Integration of antagonistic signals in the regulation of nitrogen assimilation in *Escherichia coli*. *Curr. Top. Cell. Regul.*, **36**, 31–75.
38. Muse, W.B. and Bender, R.A. (1998) The nac (nitrogen assimilation control) gene from *Escherichia coli*. *J. Bacteriol.*, **180**, 1166–1173.
39. Kharchenko, P., Church, G.M. and Vitkup, D. (2005) Expression dynamics of a cellular metabolic network. *Mol. Syst. Biol.*, **1**, 2005.0016.
40. Mao, F., Dam, P., Chou, J., Olman, V. and Xu, Y. (2009) DOOR: a database for prokaryotic operons. *Nucleic Acids Res.*, **37**, D459–D463.
41. Kudla, G., Lipinski, L., Caffin, F., Helwak, A. and Zylicz, M. (2006) High guanine and cytosine content increases mRNA levels in mammalian cells. *PLoS Biol.*, **4**, e180.
42. Gene Ontology Consortium. (2010) The Gene Ontology in 2010: extensions and refinements. *Nucleic Acids Res.*, **38**, D331–D335.
43. Huang da, W., Sherman, B.T. and Lempicki, R.A. (2009) Bioinformatics enrichment tools: paths toward the comprehensive functional analysis of large gene lists. *Nucleic Acids Res.*, **37**, 1–13.
44. Cook, P.R. (2009) A model for all genomes: the role of transcription factories. *J. Mol. Biol.*, **395**, 1–10.
45. Li, G., Ma, Q., Tang, H., Paterson, A.H. and Xu, Y. (2009) QUBIC: a qualitative biclustering algorithm for analyses of gene expression data. *Nucleic Acids Res.*, **37**, e101.
46. Zhou, F., Ma, Q., Li, G. and Xu, Y. (2012) QServer: a biclustering server for prediction and assessment of co-expressed gene clusters. *PLoS One*, **7**, e32660.
47. Li, G., Liu, B., Ma, Q. and Xu, Y. (2011) A new framework for identifying cis-regulatory motifs in prokaryotes. *Nucleic Acids Res.*, **39**, e42.